Recent developments on non-polar cubic group III-nitrides for optoelectronic applications

D.J. As*

University of Paderborn, Warburger Strasse 100, 33098 Paderborn, Germany;

ABSTRACT

Molecular Beam epitaxy (MBE) of cubic group III-nitrides is a direct way to eliminate polarization effects which inherently limit the performance of optoelectronic devices containing quantum well or quantum dot active regions. In this contribution the latest achievement in the MBE of phase-pure cubic GaN, InN, AlN and their alloys will be reviewed. A new RHEED control technique enables to carefully adjust stoichiometry and to severely reduce the surface roughness, which is important for any hetero-interface. The structural, optical and electrical properties of cubic nitrides and AlGaN/GaN will be presented. We show that no polarization field exists in cubic nitrides and demonstrate intersubband absorption at 1.55 µm in cubic AlN/GaN superlattices. Further the progress towards the fabrication of cubic GaN/AlGaN superlattices for terahertz applications will be discussed.

Keywords: cubic group III-nitrides, MBE, HRXRD, intersubband transitions, QWIPs

1. INTRODUCTION

Commercially available group III-nitride-based optoelectronic devices are grown along the polar c direction, which suffer from the existence of strong "built-in" piezoelectric and spontaneous polarization. This inherent polarization limits the performance of optoelectronic devices containing quantum well or quantum dot active regions. To get rid of this problem much attention has been focused on the growth of non- or semi-polar (Al,Ga,In)N. However, a direct way to eliminate polarization effects is the growth of cubic (100) oriented III-nitride layers. With cubic epilayers a direct transfer of the existing GaAs technology to cubic III-Nitrides will be possible and the fabrication of diverse optoelectronic devices will be facilitated. However, since cubic GaN is metastable and no cubic GaN bulk material exists in nature, heteroepitaxy with all its drawbacks due to lattice mismatch is necessary to grow this material. Due to the low lattice mismatch to cubic GaN the substrate of choice for the growth of cubic III-nitrides is 3C-SiC.

In this paper the latest achievements in the molecular beam epitaxy of phase-pure cubic GaN, InN, AlN and their alloys grown on 3C-SiC substrates is reviewed. A new RHEED control technique is presented to carefully adjust stoichiometry and to severely reduce the surface roughness. The structural and optical properties of cubic nitrides and AlGaN/GaN heterostructures will be shown. The absence of polarization fields in cubic nitrides is demonstrated and 1.55µm inter-subband absorption in cubic AlN/GaN superlattices is reported. The progress towards the fabrication of cubic GaN/AlGaN superlattices for terahertz applications will be discussed.

2. EXPERIMENTAL DETAILS

Cubic group III-nitride samples were grown on 200 µm thick, free standing 3C-SiC (001) substrates by molecular beam epitaxy (MBE) [1,2]. An Oxford Applied Research HD25 radio frequency plasma source was used to provide activated nitrogen atoms. Indium, aluminum and gallium were evaporated from Knudsen cells. Prior to growth, the 3C-SiC substrates were chemically etched by organic solvents and a buffered oxide etch (BOE) and annealed for 10 hours at 500°C. Cubic GaN layers were deposited at 720°C directly on 3C-SiC substrates. The adsorption and desorption of metal (Ga, Al) layers on the c-GaN surface was investigated using the intensity of a reflected high energy electron beam (RHEED) as a probe. The structural and morphological properties of 3C-SiC substrates and group III-nitride epilayers were measured by high resolution X-ray diffraction (HRXRD) and atomic force microscopy (AFM). Reciprocal space mapping (RSM) has been performed to determine the Al and In molar fraction and the strain in the epilayers.

* d.as@uni-paderborn.de ; phone +49 5251 60 5838; fax +49 5251 60 5843;

3. RESULTS AND DISCUSSION

3.1 RHEED control

As an important step to improve the GaN surface morphology in a systematic way, it is essential to understand the surface structure and the underlying growth process on an atomic scale. In particular, the kinetic processes of adsorption and desorption on the surface are considered as key parameters that govern the surface morphology, incorporation kinetics and consecutively the overall material quality. In MBE of GaN, two dimensional surfaces are commonly achieved under Ga-rich conditions, with theoretical [3] and experimental [4, 5] evidence suggesting that the growth front is stabilized by a metallic Ga adlayers. The optimum conditions for the epitaxial growth of c-GaN are mainly determined by two parameters, the surface stoichiometry and the substrate temperature [1]. Both parameters are interrelated; therefore an in-situ control of substrate temperature and surface stoichiometry is highly desirable. The study of the surface reconstruction by RHEED was one of the key issues in understanding the c-III nitride growth [1, 6, 7]. First principle calculations by Neugebauer et al. [8] show that all energetically favoured surface modifications of the non-polar (001) c-GaN surface are Ga-stabilized and therefore optimum growth conditions are expected under slightly Ga-rich conditions.

Figure 1 shows the RHEED intensity transient of the (0,0) reflection of the (2x2) reconstruction. After opening the Ga shutter we observe a steep linear decrease of the RHEED intensity between I_o and the kink position (I_k). The gradient of the intensity drop is related to the impinging Ga flux. Using the known value of the Ga flux and the time Δt_k it takes for the RHEED intensity to drop to I_k, we are able to calculate the amount of adsorbed gallium. Neglecting re-evaporation of Ga we get a total number of adsorbed Ga atoms from the flux time Δt_k product. In all cases this product is about 9.8 x 10^{14} cm^{-2}, which is equal the number of atoms of exactly one monolayer of Ga on the GaN surface (lattice constant of 4.52 Å). Since I_o is the reflectivity of the GaN surface and I_k is the reflectivity of GaN covered by one Ga monolayer,
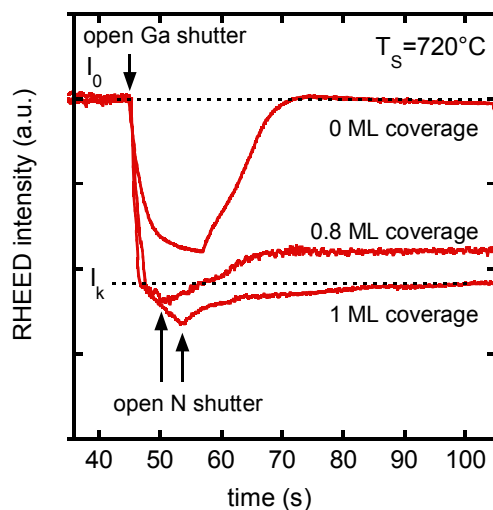

Figure 1. RHEED intensity transient measured during the growth of *c*-GaN, which started after opening the *N* source. The RHEED intensity measured during growth yields the amount of excess Ga (indicated in the figure) on the *c*-GaN surface. The Ga fluxes are 4.4x10^{14}, 3.2x10^{14}, and 1.2x10^{14} cm^{-2} for the coverages of 1, 0.8, and 0 ML, respectively.
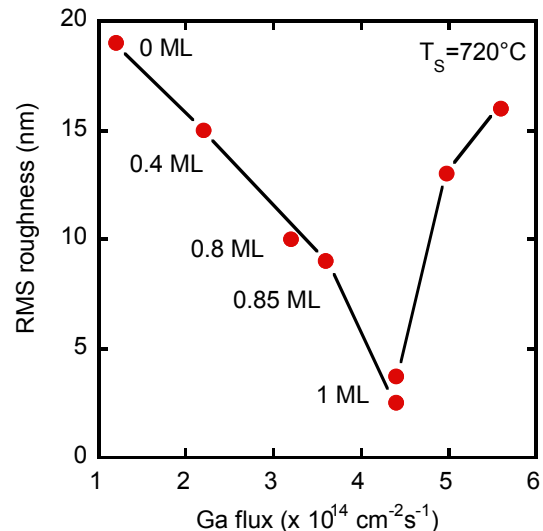
Figure 2. RMS roughness of *c*-GaN layers measured by 5x5 µm^2 AFM scans vs Ga flux during growth. The corresponding values of the Ga coverage during growth are also included. Minimum roughness is obtained with an excess coverage of 1 ML. The line is a guide for the eyes.

and the drop of the RHEED intensity in the time interval Δt_k is linear, the Ga coverage between 0 and one monolayer can be inferred from the measured intensity drop by linear interpolation. The decrease of the RHEED intensity below I_k is most likely due to further accumulation of Ga and thereby a modification of the Ga adlayer surface, however it is notproportional to the amount of adsorbed Ga. For this reason our method can only be used to measure the Ga coverage between zero and one monolayer, respectively. For Ga fluxes less than 3×10^{14} cm^{-2}s^{-1} the situation is different. For these fluxes it is not possible to define a kink position. The RHEED intensity drops to a certain value and saturates. We suppose that then desorption of Ga cannot be further neglected.

After opening the N shutter we observe an increase of the RHEED intensity which is due to the formation of c-GaN. During further growth the RHEED intensity saturates. From the saturation value the Ga coverage can be calculated using I_k as a reference. This procedure allows measuring the Ga-coverage in the range between 0 and 1 monolayer with an accuracy of 0.1 monolayer.

Figure 2 shows the root-mean-square (RMS) - roughness measured by a 5×5 μm^2 AFM-scan of several c-GaN layers versus the Ga flux used during MBE. The nitrogen flux was kept constant for all samples. The corresponding values of the Ga coverage during growth, as measured by the procedure described above, are included in Fig. 2. Only values below one monolayer can be measured. Minimum roughness is obtained with one monolayer Ga coverage during growth. This is in contrast to what has been observed with h-GaN, where the optimum growth conditions with regard to surface morphology are related to the formation of a Ga bilayer (c-plane, [9, 10]) or a trilayer (m-plane, [5]), respectively.

It has variously been suggested that excess Ga acts as surfactant during the epitaxy of hexagonal-GaN [9, 11, 12]. We believe that our data shown in Fig. 2 clearly demonstrate that this effect exists also on the (001) surface of c-GaN. The width of the (002) X-ray rocking curve measured in double axis configuration of 1μm thick c-GaN layers grown with one monolayer coverage is about 16 arcmin. Among our c-GaN layers with equal thickness 16 arcmin is a minimum value. Gallium fluxes which are equivalent to a Ga coverage exceeding one monolayer lead to a pronounced increase of the roughness and the FWHM of the X-ray rocking curve.

3.2 Cubic GaN

High-resolution X-ray diffraction (HRXRD) allows to measure the density of extended defects in epitaxial layers. The full width at half maximum (FWHM) of the Bragg reflex measured in a direction perpendicular to the diffraction vector (ω-scan) is related to the intensity of extended defects in the layer. The ω-scan measures the intensity spread for the coordinate $q_\perp$ in reciprocal space arising from both mosaicity and finite lateral domain size. Fig. 3 compiles HRXRD data from c-GaN layers with a varying thickness grown by MBE on GaAs [13,14] and 3C-SiC [15] substrates, respectively. A clear decrease of the FWHM with increasing layer thickness is seen and the values given in Reference [14] are quite comparable to our data. The linewidths measured for c-GaN grown on 3C-SiC substrates are approximately a factor of three narrower than that for layers grown on GaAs substrates. This may be expected due to the lower lattice mismatch of this system. The clear trend of decreasing FWHM with increasing layer thickness inmediately implies that the number of extended defects is reduced in thicker epilayers.

In Fig. 3 the rocking curve line width (ω-scan) of all our cubic GaN epilayers (full triangles) grown on 3C-SiC is plotted versus c-GaN layer thickness. Two effects can clearly be seen from this plot. First a severe reduction of the full width at half maximum (FWHM) with increasing epilayer thickness is observed. This linewidth dependence is consistent with the defect annihilation process observed in cubic GaN grown on GaAs (001) substrates [16]. Since in zinc-blende structure the stacking faults (SFs) lie on the (111) planes, an annihilation mechanism is possible, when two SFs, lying, for example on the (111) and on the (-1-11) planes intersect and annihilate simultaneously with the creation of a sessile dislocation aligned along [110] directions. For the case of 3C-SiC, where the lattice mismatch is only -3.7 % to cubic GaN, the full line shows the theoretical calculated FWHM as a function of layer thickness using the dislocation glide model by Ayers [17]. This model implies that the dislocation density N_{disl} is inversely proportional to the layer thickness d and that the FWHM is proportional to $d^{-1/2}$. In addition with this model order of magnitude accuracy in quantiative predictions of the dislocation densities for a number of heteroepitaxial systems can be achieved. The full line through the 3C-SiC data shows this model calculation, which gives a relation between the dislocation density N_{disl}, the lattice misfit between substrate and epitaxial layer and the thickness of the epilayer. In the calculation it was assumed that 60° dislocations with a Burgers vector of 0.32 nm are the predominant defects in the layers. The trend of the calculated curve is in excellent agreement with the experimental data. The estimated dislocation density N_{disl} is shown on the right hand

scale of the diagram. Comparing the full curve with the experimental data (full triangles) a reduction of the FWHM by a factor 1.5 is still possible. By comparing our data with data cited in literature the dependence of the FWHM on film thickness has to be taken into account. Up to now, only two other groups reported data on GaN on 3 - 5 μm thick

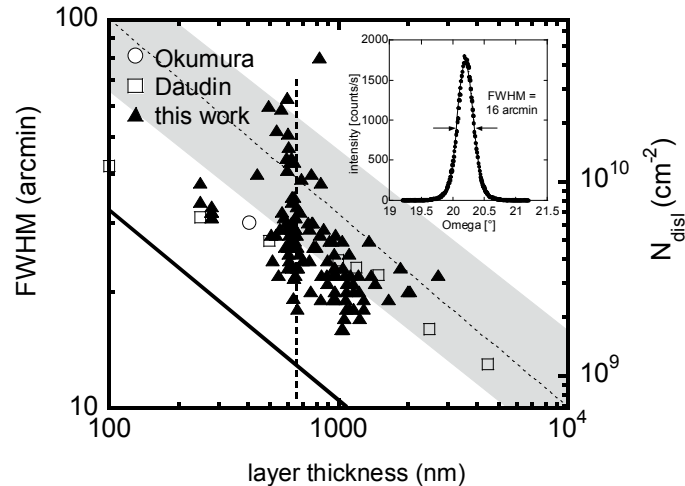Figure 3. Rocking curve linewidth of cubic GaN epilayers grown on 3C-SiC substrates versus thickness of the cubic epilayers.

3C-SiC/Si (001) pseudo-substrates grown by chemical vapor deposition (open circle Ref. [18] and open squares Ref. [15]). As can be seen in Fig.3 we clearly are able to remain under the best cited values, indicating the improved structural quality of our c-GaN epilayers due to the availability of free standing, bulk like 3C-SiC (001) substrates. The HRXRD data are in good agreement with TEM investigations [14] which yield a defect density in the order of 10^9 to 10^{11} cm^{-2}. In addition, TEM measurements further showed that the density of stacking faults is drastically decreasing with increasing layer thickness. As mentioned above, the second parameter which strongly influences the quality of the cubic epilayers is the roughness of the 3C-SiC substrate. In Fig. 3 the linewidth of the rocking curve of 600 nm thick cubic GaN epilayers on 3C-SiC substrates varies from 60 arcsec to 20 arcsec for substrates with different surface roughness (indicated by the vertical dashed line). The root mean square (RMS) roughness of the corresponding 3C-SiC substrates as measured by AFM on 5 x 5 μm^2 large areas varied between 11 nm and 0.7 nm, respectively. The smoother the surface of the substrates the narrower is the FWHM and the higher is the structural quality of the cubic epilayer. This observation is in agreement with measurements of Ref. [18] and indicates that a further improvement of the surface preparation (atomic flat surfaces) may allow to reach the theoretical limit indicated by the full line. Up to now, the X-ray rocking curve of a 1μm thick c-GaN layer grown with 1 monolayer coverage was about 16 arcmin (see inset of Fig. 3), which to our knowledge is one of the best values reported so far.

For the sake of completeness the shaded area in Fig. 3 depicts the range of FWHM values as measured for cubic GaN grown on GaAs substrates. However, the model of Ayers cannot be applied to heteroepitaxial systems with mismatch greater than about 10 % since in such systems the misfit dislocations are so closely spaced that the continuum elasticity theory cannot predict their line tension with acceptable accuracy. However, if we shift the calculated line upwards, one sees that for the c-GaN/GaAs case the same trend is observed (dashed line through shaded area). Therefore we think that the same defect annihilation process is also effective in the GaAs case. From the right hand scale we estimated a dislocation density of about 10^{10} cm^{-2} for a 1 μm thick c-GaN epilayer on GaAs (001).

However, it is well known that hexagonal inclusions mainly grow on (111) facets and cannot be detected by ω–2Θ–scans. Therefore reciprocal space maps (RSM) of the GaN (002) Bragg-reflex were performed. The RSM of an 600 nm thick cubic GaN epilayer on 3C-SiC substrate along the (-110) azimuth is shown in Fig. 4. Only a very weak intensities of the (10-11) and (-1011) reflexes from hexagonal GaN (indicated in Figure 4 by arrows) is measured yielding a content of hexagonal inclusions below 1 %.
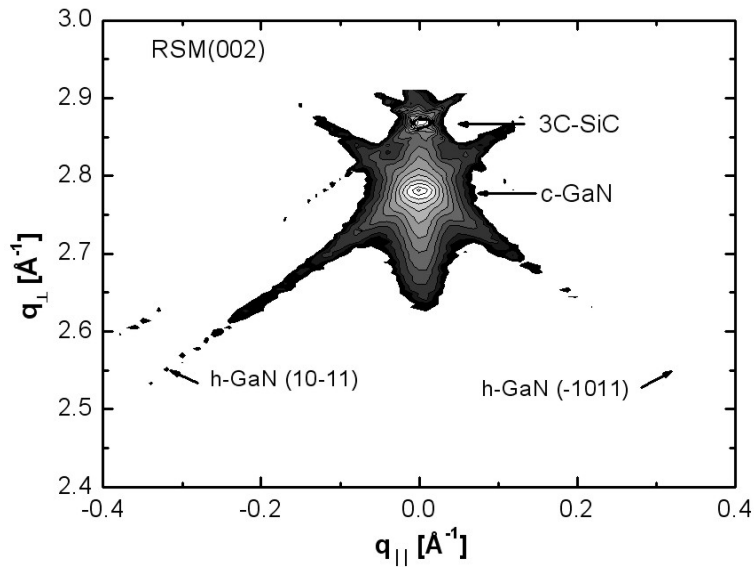
Figure 4. Reciprocal space map of a 600 nm thick cubic GaN epilayer grown on 3C-SiC substrates. High intensity (002) Bragg relexes of c-GaN and the 3C-SiC substrate are observed. Only a very weak (10-11) reflex from hexagonal GaN is measured yielding a content of hexagonal inclusions below 1 %.

Figure 5 shows the photoluminescence spectrum at 2 K in a semilogarithmic plot for a 0.8 µm thick stoichiometrically grown c-GaN epilayer deposited on a (001) 3C-SiC substrate. The near band edge spectral range is dominated by two well resolved peaks at about 3.26 eV and 3.15 eV with a full-width at half maximum (FWHM) of 11 meV and 43 meV, respectively. Temperature dependent measurements of these two lines allow to assign the 3.26 eV emission to radiative recombination of an acceptor bound excitons (A^o,X) and the 3.15 eV line to a donor-acceptor recombination (D^o,A^o) [19]. Above 3.3 eV, which is the value of the low temperature gap energy of the cubic GaN measured by photoreflection [20], the PL-intensity drops by more than three orders of magnitude. In this spectral region we find no trace of near-band-edge or defect-related [21] emission lines from inclusions of hexagonal crystal structure.

In the energy range below 3.1 eV further optical transitions can be observed in the PL-spectrum of different samples. With decreasing energy the transitions occur at 3.07 eV, 3.03 eV, 2.97 eV, 2.85 eV, 2.65 eV and 2.4 eV. The intensity of these peaks are by more than one order lower than that of the dominating (D^o,A^o) transition and vary significantly between different samples. Temperature dependent measurement of these lines show no characteristic 25 meV shift as it has been observed for the 3.15 eV (D^o,A^o) transition. For that reason, these lines are either band-acceptor (e,A^o) or donor-hole (D^o,h) transitions. Due to the larger binding energies of the involved defects the corresponding wavefunctions may be strongly localized. This reduces the recombination probability for donor-acceptor transitions and favours the band-impurity transition. Using a band gap energy of 3.302 eV [20] the energy levels of the defects are estimated to be 0.232 eV, 0.272 eV, 0.332 eV, 0.452 eV, 0.652 eV, and 0.902 eV above the valence band or below the conduction band of c-GaN, respectively. Similar defects in c-GaN have also be seen by N.N. Zinov´ev et al. [22].

Additional valuable information about the electronic band structur of cubic GaN epilayers can be provided by studying the temperature and pressure dependence of the optical transitions in semiconductors [19, 23]. At temperatures above 100 K the peak position of the exciton line follows exactly the energy gap measured by photoreflectance [20]. Assuming an exciton binding energy of $E_{exc} = 26$ meV excellent agreement is found between the experimental data and the temperature dependence of the exciton emission energy above 100 K. The 13 meV deviation at low temperatures is attributed to an increasingly stronger contribution of bound exciton transitions. Using Haynes rule [24], which has been confirmed in hexagonal GaN [25], and assuming that the excitons are bound to acceptors, we obtain an acceptor ionization energy of about 130 meV. This agrees well with the acceptor binding energy evaluated from the (D^o,A^o)

transition. Using a donor and acceptor energy of 25 meV and 130 meV, respectively, and the temperature dependence of the energy gap [20] a temperature dependent emission energy of the (e,A^o) and the (D^o,A^o) transitions are obtained. The good agreement with the experimental data supports the interpretation that in the cubic epilayers a shallow donor with $E_D = 25$ meV and an acceptor with $E_A = 130$ meV are involved in the observed near-band photo-luminescence.
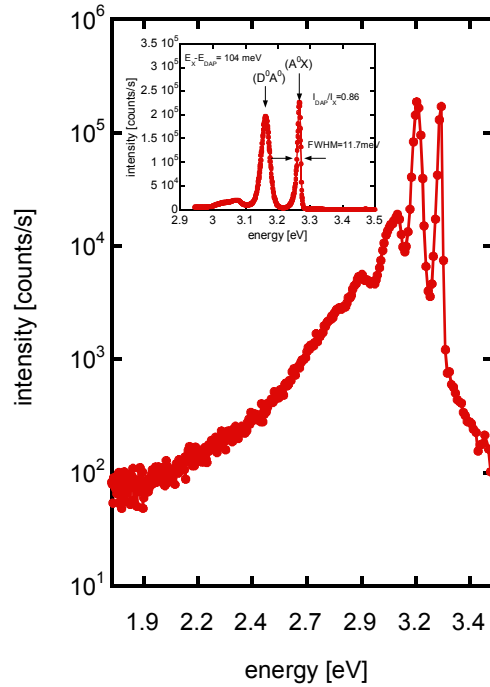

Figure 5. Low temperature photoluminescence spectrum of cubic GaN epilayers grown on 3C-SiC substrates (logarithmic scale). In the inset the band edge region is plotted in a linear presentation.

The dominating near band transitions $((D^0,A^0)$, (A^o,X) lines) are observed in all cubic GaN epilayers independent of the growth technique used and also independent of the substrates used. Therefore, the ratio of the PL-intensities of the (D^0,A^0) and bound exciton (A^o,X) lines is often taken as a measure for the quality of the epilayers [26]. However, since the nature of these two transitions is different the intensity ratio depends on the excitation intensity conditions. Recently, Daudin et al. [18] also showed that the ratio of these lines depends strongly on the Ga/N flux ratio and increases for Ga-rich conditions. Therefore, it is not possible to use this ratio to compare different samples grown by different growth techniques if they are grown at different laboratories.

3.3 Cubic InN

Among nitride semiconductors, InN is the least investigated of all and is expected to be a promising material for high frequency electronic devices [27, 28]. The most important recent discovery about InN is that it has a much narrower band-gap than reported previously. For h-InN values between 0.6 eV and 0.7 eV are measured [29, 30]. Group III-nitrides with cubic crystal structure are expected to have even lower band gaps and can be grown on substrates with cubic structure. However, the zinc-blende polytype is metastable and only a very narrow growth window is available for the process conditions [1].

Cubic InN films were grown on top of a c-GaN buffer layer (600 nm). The c-GaN buffer layer was deposited on free standing 3C-SiC (001) substrates at growth temperatures of 720 °C. For the InN growth the temperature was reduced and varied in the range of 419°C to 490°C, respectively. InN growth was started under In rich conditions at an In-BEP of

6.8*10⁻⁸ mbar which was decreased to 3.1*10⁻⁸ mbar after two minutes of growth. The thicknesses of the InN layers were at least 130 nm and the growth was continuously monitored by RHEED.

HRXRD investigations were performed to determine the phase purity of our c-InN layers. All $\omega-2\Theta-$scans confirmed the formation of the cubic phase of InN. Bragg peaks observed at 35.8°, 39.9° and 41.3° correspond to c-InN (002), c-GaN (002) and 3C-SiC (002), respectively. No additional reflection of h-InN grown in (0002) direction was detected. The full width at half maximum (FWHM) of the (002) rocking curve was 48 arcmin. The lattice constant derived from the $\omega-2\Theta-$scan is 5.01 Å +/– 0.01 Å in good agreement to the values published [9]. However, as mentioned above hexagonal inclusions mainly grow on (111) facets and cannot be detected by $\omega-2\Theta-$scans. Therefore reciprocal space maps (RSM) of the GaN (002) Bragg-reflex were performed. The RSM along the (-110) azimuth is shown in the inset of Fig. 6. The growth temperature of this InN sample was 419°C. From the intensity ratio of the cubic (002) reflex to the hexagonal (10-11) reflex we estimate 95 % cubic phase in this InN layer. A RSM of the asymmetric GaN (-1-13) reflex shows, that the lattice of our c-InN layers is fully relaxed with respect to the c-GaN buffer.

In Fig. 6 we plot the ratio of the intensities of the h-(10-11) Bragg reflex and the c-(002) reflex versus the growth temperature of different InN layers. We observe a strong decrease of hexagonal inclusions with decreasing growth temperature up to a minimum value of 5 %. This supports the idea that with decreasing growth temperature the sticking coefficient of In is increased, resulting in a higher density of cubic nuclei on the surface, which reduce the formation of (111) facets.

The low temperature PL spectrum of an InN layer grown at 419 °C shows a peak at about 0.69 eV with a FWHM of 170 meV [31]. We suppose that the broadening of the luminescence is due to the fact that the c-InN is degenerated. The high electron densities above 10^{19} cm⁻³ cause pronounced Burstein–Moss shifts at the gap. Taking into account non-parabolicity and band filling effects, data analysis yields renormalized band edges $E_g(n)$ close to 0.61 eV at low temperature for c-InN. Subtracting a temperature shift of about 50 meV between 10 K and 300 K the band-gap of c-InN is about 0.56 eV at room temperature. This value is in excellent agreement with measurements of the complex dielectric function for cubic InN by spectroscopic ellipsometry (SE) from the mid-infrared into the visible spectral region. From SE a zero-density band gap of ~0.595 eV is estimated for c-InN. Therefore, the band gap of cubic InN is about 85 meV lower than that for hexagonal InN [32].
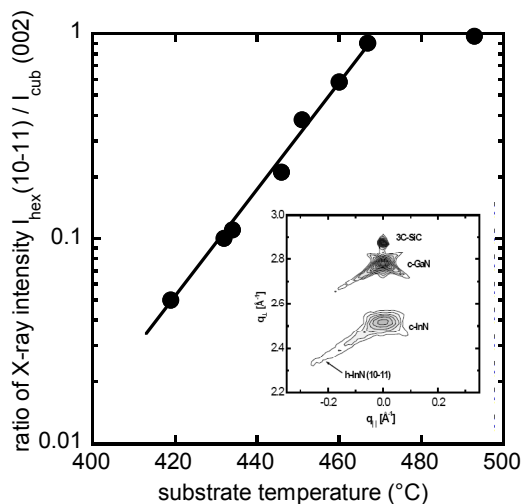
.

Figure 6. Intensity ratio of the (10-11) reflex of hexagonal inclusions to the (002) Bragg reflex of cubic InN versus growth temperature of c-InN layers. The inset shows the reciprocal space map for the c-InN sample grown at 419°C.
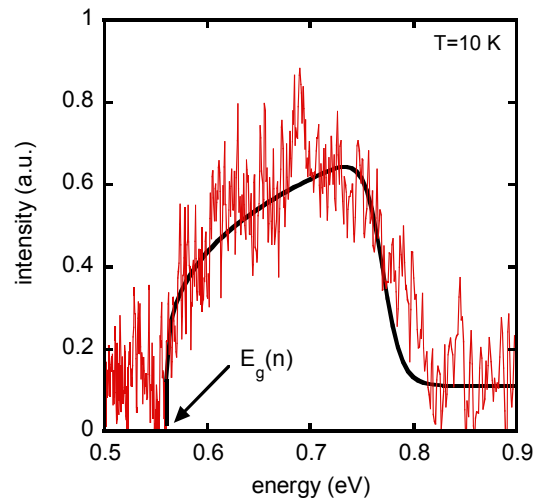
Figure 7. Low temperature photoluminescence of a cubic InN sample grown at 419°C.

A pronounced difficulty in the determination of the electrical properties of InN is due to the fact that electron accumulation is found to occur at the surface of wurtzite InN. Using x-ray photoemission spectroscopy a similar accumulation effect is also demonstrated for cubic InN [33]. The surface Fermi level pinning was shown to be the same for *a*-plane and for both polarities of *c*-plane wurtzite InN, although the pinning was slightly lower for zinc-blende (001) InN. This is due to the low Γ-point conduction band minimum lying significantly below the charge neutrality level. Therefore, the accumulation is shown and the accumulation seems to be a universal feature of InN surfaces.

3.4 Cubic InGaN/GaN Quantum Wells

For optoelectronic devices like high efficient green or blue LEDs $In_yGa_{1-y}N$/GaN quantum wells are the key elements in the active zones. In hexagonal $In_yGa_{1-y}N$/GaN MQWs, which are mainly grown in a (0001) growth direction, strong built-in electric fields due to the piezoelectric effect and spontaneous polarization severely reduce the radiative recombination efficiency for wider QWs [34]. For that reason, the optimal thickness of h-InGaN well is around 2-3nm in the h-InGaN/GaN system. Due to the higher crystal symmetry polarization fields are absent in cubic III-nitrides and due to the slightly smaller energy gap of the cubic nitrides (200 meV lower than the hexagonal counterpart), smaller mole fractions of In in the well of $In_yGa_{1-y}N$/GaN quantum wells are necessary to reach emission wavelengths beyond 510 nm.

We have grown a 6-fold c-$In_yGa_{1-y}N$/GaN MQW on 3C-SiC substrates [35]. Figure 8 shows a typical XRD reciprocal space map around the (-1-13) reflection on c-$In_yGa_{1-y}N$/GaN MQW. The superlattice peaks are clearly resolved up to the 5th order and the $In_yGa_{1-y}N$ wells are pseudo-morphically grown on the GaN barrier layers. From the X-ray diffraction data an $In_yGa_{1-y}N$ well thickness of 5.6 nm and a GaN barrier thickness of 12.1 nm are obtained. The In mole fraction is about 0.16. The strong and dominant room temperature 2.4 eV (510nm) MQW emission is shown in Fig. 9. The GaN emission can not be detected, revealing a high radiative recombination efficiency of the InGaN quantum wells. These properties indicate that cubic $In_yGa_{1-}N$/GaN MQWs seem to be the material of choice for the realization of resonant cavity light emitting diode (RC-LED) for the 500–570 nm spectral range [36].
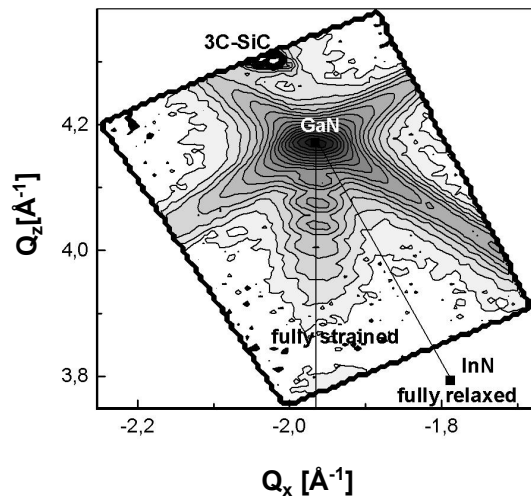

Figure 8. High resolution XRD reciprocal space map near (-1-13) reflection of a 6 fold cubic $In_{0.16}Ga_{0.84}N$/GaN MQW grown on free standing 3C-SiC substrates. Arrow indicates 5th order superlattice peak.
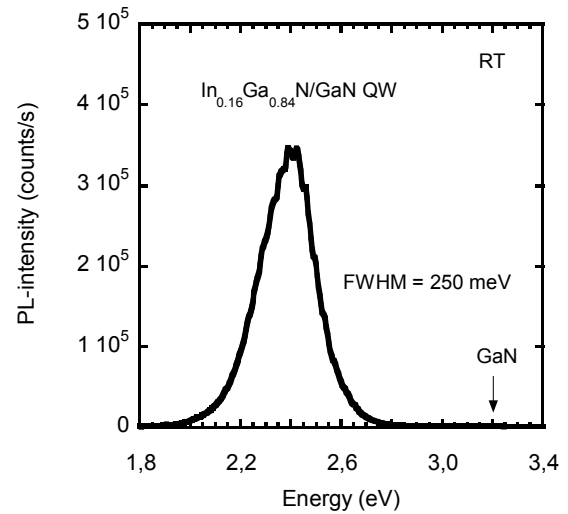
Figure 9. Room temperature PL spectrum of a 6 folds cubic $In_{0.16}Ga_{0.84}N$/GaN MQWs.

3.5 Cubic AlN

AlN is a group III nitride wide-band gap semiconductor with a large thermal conductivity comparable to copper, a hardness close to sapphire and a high chemical stability. Until recently the meta-stable cubic phase of AlN had a considerable surface roughness, leading to short-circuits and broadening of confined electronic states of low dimensional structures [37,38]. However. the PAMBE growth of atomically flat c-AlN layers on freestanding 3C-SiC substrate was reported by us recently [39]. The growth procedure started with a deoxidation of the substrate. Surface oxides lead to blurred reflections of the cubic lattice, three dimensional islands on the surface cause disc shape reflections due to an electron transmission component [40]. After cleaning the RHEED pattern of the 3C-SiC surface shows long thin streaks indicating a two dimensional oxide free surface with a (2x4) reconstruction and Kikutchi lines. The used cleaning process can be found in more details in Ref. 39.

Due to its metastable nature, exposing a c-AlN surface to nitrogen lead to the formation of hexagonal clusters. However, growing c-AlN with one monolayer Al surface coverage can prevent hexagonal condensation [39,31]. Therefore, the c-AlN nucleation on the 3C-SiC substrate was done under one monolayer (ML) of Al surface coverage. The substrate temperature was 730°C and the Al beam flux was $2*10^{14}$ cm^{-2}s^{-1}, respectively. The growth was monitored *in-situ* by RHEED. At the initial growth process a transition from a 2D to a 3D surface was observed. This transition is clearly seen in Fig. 10 if we compare the RHEED pattern after the deposition of 6 ML of c-AlN (Fig. 10(a)) with that after deposition of 30 ML (Fig. 10 (b)). The spotty reflections originating from an electron transmission component through islands on the surface are transformed into long streaks. After a smooth surface was established, growth interruptions of 30 seconds were applied every 20 atomic layers to avoid metal accumulation at the surface. RHEED intensity oscillations (not shown here) indicate a two-dimensional layer-by-layer growth and the growth rate was determined to be 0.2 ML/s. A smooth 2D surface is still seen after the growth of 142 nm (650 ML) c-AlN (see RHEED pattern in Fig. 10(c)).
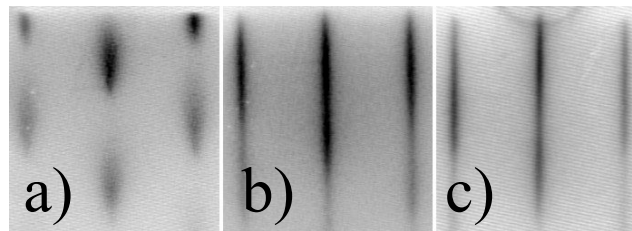

Figure 10. RHEED images of the c-AlN surface during the initial growth process. (a) after growth of 6 ML, (b) after growth of 30 ML, (c) after growth of 650 ML.

The cubic structure of the AlN layer is clearly shown by HRXRD measurements. In Fig. 11 the HRXRD (113) reciprocal space map of a 300 nm c-AlN layer on 3C-SiC is shown. The peak of the arrow 3 indicates the position of the 3C-SiC Bragg reflection, the peak of arrow 1 indicates the position of the c-AlN reflection. The elliptic shape originates from a mosaic structure caused by strain relaxation [41]. The main axis of the ellipse (white line in Fig. 11 labelled by 4) is perpendicular to the reciprocal lattice vector. A small shift of the c-AlN peak along the main axis can be interpreted as tilt of the c-AlN layer versus the substrate. Taking this tilt into account the position of the c-AlN reflection is shifted to the peak position indicated by arrow 2. The c-AlN lattice parameter in growth direction extracted from Fig. 11 is 4.373 Å +- 0.002 Å.

The high surface quality of the c-AlN layers is verified with AFM. The AFM image of the c-AlN layer shows an atomically smooth surface with a roughness of 0.2 nm RMS. The according line scan depicts a peak-to-valley height of only 1 lattice constant over a lateral extension of ~ 2000 lattice constants.

A commercial ellipsometer was employed for recording the ellipsometric parameters Ψ and Δ under different angles of incidence (Φ: 60°, 67°, and 74°) in the photon (ℏω) energy range from 1 to 6.4 eV. A home-made construction attached to the Berlin Electron Storage Ring for Synchrotron Radiation (BESSY II) allowed measurements of Ψ and Δ under Φ=67.5° from 5 to 10 eV with the set-up described in Ref. 42. The dielectric function (DF) was obtained by a multi-layer fitting procedure similar to the approach presented in Ref. 43. No assumption was made concerning the shape of the DF,
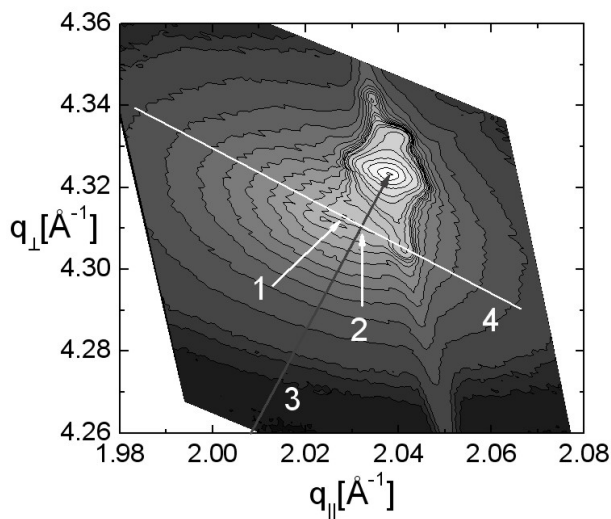
Figure 11. HRXRD reciprocal space map of the (113) reflections of c-AlN and 3C-SiC. (1) position of the c-AlN peak, (2) position of c-AlN peak after tilt correction, (3) reciprocal lattice vector of 3C-SiC reflection, (4) axis for tilt correction perpendicular to (3).

i.e. the real (ε_1) and imaginary parts (ε_2) of the DF were separately fitted for all photon energies. Figures 12 a) and b) summarize the results of the fitting procedure for one of the cubic AlN films (layer thickness here was 100 nm). The spectral dependence shows similarities to the recently reported results for the hexagonal counterpart [44] however, the characteristic energies E_0, E_1, and E_2 differ appreciably.
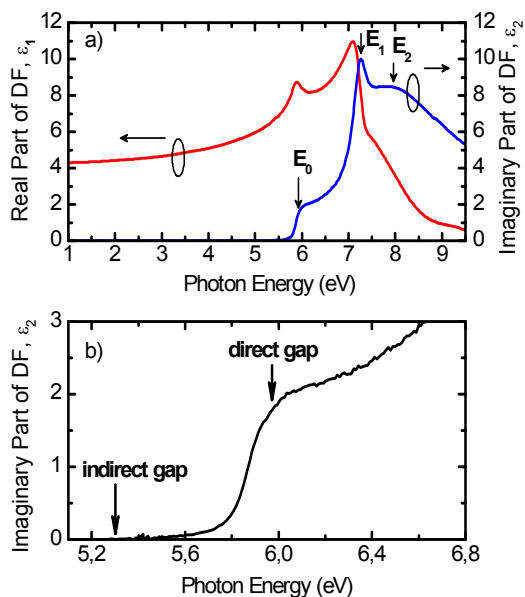

Figure 12. a) Real and imaginary part of the DF for c-AlN from 1 to 10 eV. b) Magnification of the region close to the absorption edge.

The imaginary part of the DF exhibits a sharp onset at 5.88 eV which defines the direct excitonic band gap. Adopting the exciton binding energy of 50 meV for the hexagonal AlN [45] we determine the direct band gap (E_0) at the Γ point of the Brillouin zone with 5.93 eV. This result is in excellent agreement to the calculated quasi-particle band gap of 5.86 eV if the lattice polarizability is taken into account [45]. For comparison, previous studies of mixed phase AlN yielded 5.74 eV for the zinc-blende compound [46]. The pronounced absorption tail below 5.88 eV in Fig. 5b) is attributed to phonon-

assisted indirect absorption. The imaginary part differs appreciably from zero only above 5.3 eV, i.e. this energy defines the upper limit of the indirect band gap. A slightly lower value might be possible as well, but ellipsometry is not sensitive enough in the case of low absorption. Finally, the E_1 and E_2 transition energies at room temperature amount to 7.20 and 7.95 eV, respectively. More results on the optical characterization are published elsewhere [44].

Atomically smooth c-AlN layers on 3C-SiC substrate have been grown by PAMBE. AFM scans and RHEED patterns verified the smooth surface. HRXRD measurements confirmed the cubic structure of the c-AlN layers with a lattice parameter of 4.373 Å. Finally, we determined the dielectric function of c-AlN over a large spectral range yielding the direct and indirect band-gap energies at 5.93 eV and about 5.3 eV, respectively.

3.6 Cubic AlGaN/GaN Quantum Wells

Cubic $Al_xGa_{1-x}N$ epilayers and cubic $Al_xGa_{1-x}N$/GaN MQW have been grown by MBE at 720°C. Such Al containing epilayers are necessary for cladding layers in laser diodes or LEDs and are also used in resonant cavity LEDs for the realization of $Al_xGa_{1-x}N$/GaN distributed Bragg reflectors.

Figure 13 shows the XRD ω-2Θ scan of the (002) Bragg-reflection of a 15 period $Al_xGa_{1-x}N$/GaN MQW structure (upper curve). The reflections of the 3C-SiC substrate, of the c-GaN buffer as well as several superlattice peaks (SL-5 to SL+2) are clearly seen. This indicates a good $Al_xGa_{1-x}N$/GaN interface quality. The experimental data have been fitted using dynamic scattering theory (lower curve), yielding a well width of 10.2 nm, a barrier width of 10.8 nm and an Al mole fraction of x=0.3. These values are in excellent agreement with data, which were obtained from growth rate measurements using RHEED oscillation period. The appearance of RHEED oscillations after opening the Al shutter [40] emphasizes a two dimensional $Al_xGa_{1-x}N$ growth mode at substrate temperatures of 720°C.
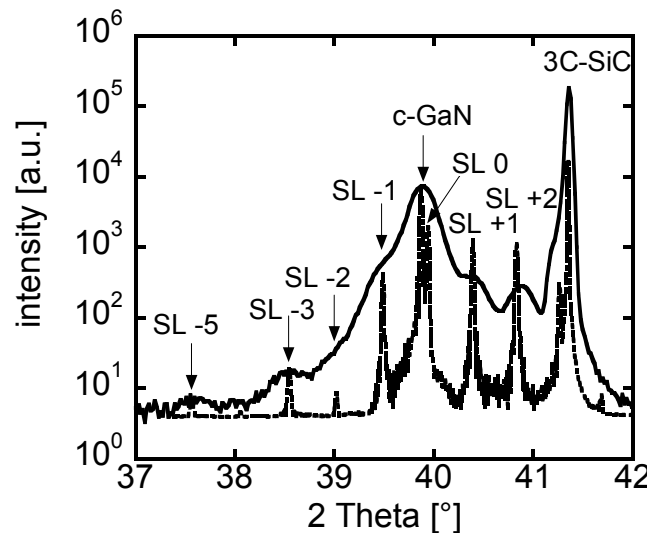

Figure 13. Measured ω–2Θ scan of 15 x $Al_{0.3}Ga_{0.7}N$/GaN MQW structure (solid line) and simulated data (dotted line). The well and the barrier width are 10.2 nm and 10.8 nm, respectively.

To demonstrate the absence of internal spontaneous polarization fields in the cubic group III-nitrides cubic single and multi $Al_{0.15}Ga_{0.85}N$/GaN quantum wells were grown on 3C-SiC/GaN substrates [47]. The quantum structures consist of 6 nm thick $Al_{0.15}Ga_{0.85}N$ barriers and GaN wells with a width of 2.5 –7.5 nm and were sandwiched between 50 nm AlGaN cladding layers. During growth of $Al_{0.15}Ga_{0.85}N$/GaN QWs clear RHEED oscillations were observed allowing a stringent control of the growth rate and indicating two dimensional growth of the respective layers. The room temperature photoluminescence spectra of a multi quantum well (MQW) structure excited with a HeCd-UV laser is shown in the inset of Figure 14. The dimensions of the quantum structures are 3 nm thick wells and 6 nm barriers. We observe a strong emission at 3.30 eV, which lies between the c-GaN emission at 3.2 eV and the emission of the $Al_{0.15}Ga_{0.85}N$ cladding layer at about 3.48 eV [48]. The PL linewidth of cubic QW luminescence is about 103 meV and is almost comparable to values reported for non-polar hexagonal AlGaN/GaN quantum wells [49]. We attribute the slightly broader linewidth in the cubic structures to the higher density of dislocations.

Figure 14 depicts the dependency of the QW emission energy on the well width for both cubic (blue squares) and hexagonal QWs (red dots). Therein, the shift in transition energies compared to the band gap energy is plotted versus well width. For our cubic $Al_{0.15}Ga_{0.85}N/GaN$ QWs the peak energy of the emission exactly follows the square-well Poisson-Schrödinger model and demonstrates the absence of polarization induced electrical fields. For comparable hexagonal $Al_{0.17}Ga_{0.83}N/GaN$ QWs on sapphire substrates the experimental data can only be explained if an internal spontaneous electrical field of 750 kV/cm is taken into account [50]. These results indicate that the well known thermodynamic metastability of the cubic nitrides does not necessarily limit their application for polarization free structures.
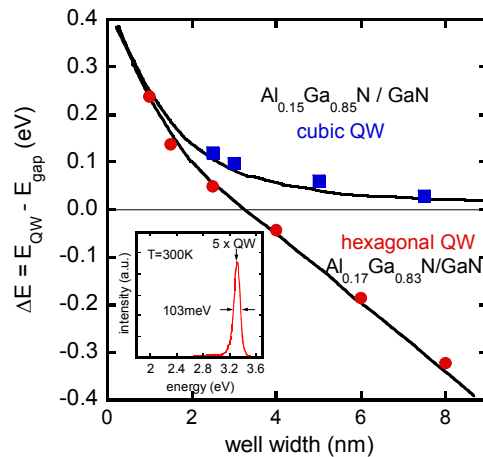

Figure 14. Transition energies of $Al_{0.15}Ga_{0.85}N/GaN$ MQWs versus well width for cubic (blue squares) and hexagonal (red dots) MQWs. The squares and dots are experimental data; the curves are calculated using a self-consistent Poisson-Schrödinger model. For the hexagonal QWs an internal field of 750 kV/cm is estimated. Inset: Room temperature photoluminescence spectrum of a cubic MQW.

3.7 Intersubband transition in cubic AlN/GaN superlattices

Intersubband transitions form the basis for quantum well infrared photodetectors (QWIP) and quantum cascade lasers (QCL). Due to the wide band gaps and the large band offsets between AlN and GaN this group of III-Nitrides offer intersubband transitions in the technologically important infrared 1.3-1.5 µm spectral range. The growth of non-polar cubic GaN/AlN multi quantum well (MQW) structures on (001) oriented substrates will eliminate the detrimental strong spontaneous polarization fields, allowing easier design of the complex MQW structures with various quantum well widths as it is necessary for the QCL systems.

Cubic GaN/AlN short period multi quantum well structures were grown at 720°C by using plasma-assisted molecular beam epitaxy on free standing 3C-SiC substrates [51]. The buffer layer was 100 nm thick GaN and the active region was composed of 20 periods of L_W GaN/1.5nm AlN, where L_W is the well thickness between 1.6 nm – 2.10 nm. The active region is then capped by a 100 nm thick GaN. The structural properties were measured by HRXRD. From the difference of the superlattice peaks in the ω-2Θ scan of the (002) reflection a periodicity of 3.1 nm was estimated by using a dynamic simulation program for a 20 period GaN/AlN MQW structure. From the knowledge of the growth rates of AlN and GaN, obtained from RHEED oscillations, a barrier and well width of 1.35 and 1.75 nm is determined, respectively.

In Figure 15 the optical absorption spectra of the intersubband transitions measured at room temperature is shown for four different MQW samples with well widths ranging between 1.60 nm to 2.10 nm. All four samples exhibit strong absorption peaks in the spectral range of 1.5 -2 µm. In the inset of Fig. 15 the measured intersubband transition peak position energies (red circles) and the calculated (solid black line) transition energies using a square well self-consistent Poisson-Schrödinger model are depicted. It is clear from this figure that good agreement is obtained between theory and experiment.
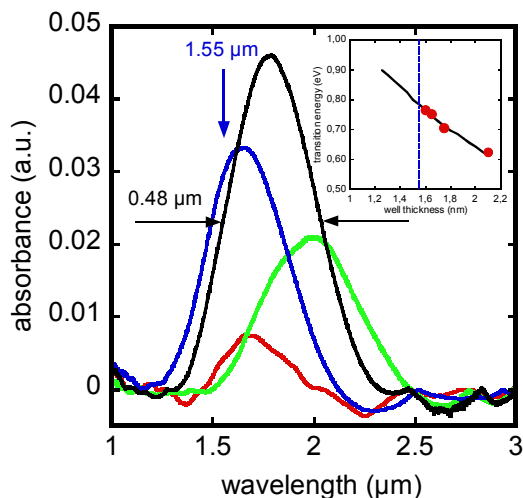
Figure 15. Optical absorption spectra of the intersubband transitions in cubic GaN/AlN short period mult quantum wells (MQWs). Inset: Intersubband transitions energy vs. well width. Circles are the experimental data and the solid line is the results of the theoretical calculations.
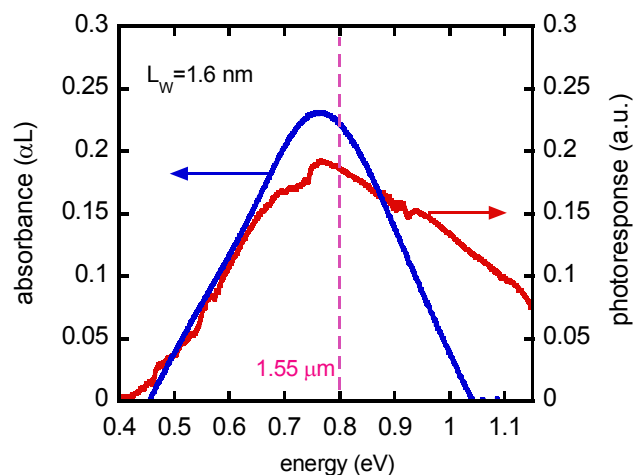
Figure 16. Optical absorption and photo-response spectra of the intersubband transitions in cubic GaN/AlN short period multi quantum wells (MQWs) at 77 K.

Recently, photo-detectors based on intersubband transitions in molecular-beam epitaxially grown cubic GaN/AlN multi quantum wells were fabricated and tested [52]. The samples were polished into waveguide configuration on which the devices were fabricated and the photo-response spectra were collected in the temperature range of 77K - 215K under the influence of small bias voltages. All devices exhibit an photovoltaic effect where the photo-response is observed at zero bias voltage. Fig. 16 shows both the optical absorbance and the photo-response at 77 K of a cubic 1.6nm/1.44nm GaN/AlN short-period multi quantum well at 1.55 µm.

4. CONCLUSIONS

Cubic GaN, InN and AlN epilayers and cubic $Al_xGa_{1-x}N$/GaN and $In_yGa_{1-y}N$/GaN MQWs were grown by plasma assisted molecular beam epitaxy on 200 µm thick free standing 3C-SiC substrates. The influence of the surface roughness of the 3C-SiC substrates and the influence of metal coverage during growth are studied in detail. Optimum growth conditions of c-III nitrides were found, when one monolayer Ga coverage is formed at the growing surface. X-ray diffraction revealed superlattice peaks up to the 5th order indicating smooth interfaces. The improvement of the structural properties of cubic III-nitride layers and multilayers grown on 3C-SiC substrates is demonstrated by a 1 µm thick c-GaN layer with a minimum x-ray rocking curve width of 16 arcmin, and by c-AlGaN/GaN and c-InGaN/GaN MQWs which showed up to five satellite peaks in X-ray diffraction. These results demonstrate that due to the availability of free standing, bulk like 3C-SiC (001) substrates and the improved structural quality of our cubic group III-nitride epilayers the way for future realization of optoelectronic devices is also opened for cubic nitrides.

REFERENCES

[1] As, D.J., in *Optoelectronic Properties of Semiconductors and Superlattices*, edited by M. O. Manasreh (Taylor & Francis, New York, 2003), Vol.19, Chap. 9, pp. 323–450

[2] As, D.J., Potthast, S., Schörmann, J., Li, S.F., Lischka, K., Nagasawa, H., Abe, M., Mater. Sci. Forum **527**, 1489 (2006).

[3] Northrup, J.E., Neugebauer, J., Feenstra, R.M. and Smith, A.R., Phys. Rev. B **61**, 9932 (2000).

[4] Koblmüller, G., Brown, J., Averbeck, R., Riechert, H., Pongratz, P. and Speck, J. S., Appl. Phys. Lett. **86**, 041908 (2005).

[5] Brandt, O., Sun, Y. J., Däweritz, L. and Ploog, K.H., Phys. Rev. B **69**, 165326 (2004).

[6] Schikora, D., Hankeln, M., As, D.J., Lischka, K., Litz, T., Waag, A., Buhrow, T. and Henneberger, F., Phys. Rev. B **54**, R8381 (1996).

[7] Feuillet, G., Hamaguchi, H., Ohta, K., Hacke, P., Okumura, H. and Yoshida, S., Appl. Phys. Lett. **70**, 1025 (1997)

[8] Neugebauer, J., Zywietz, Z., Scheffler, M., Northrup, J.E. and Van der Walle, C.G., Phys. Rev. Lett. **80**, 3097 (1998).

[9] Mula, G., Adelmann, C., Moehl, S., Oullier, J. and Daudin, B., Phys. Rev. B **64**, 195406 (2001).

[10] Adelmann, C., Brault, J., Jalabert, D., Gentile, P., Mariette, H., Mula, G. and Daudin, B., J. Appl. Phys. **91**, 9638 (2002).

[11] Gogneau, N., Sarigiannidou, E., Monroy, E., Monnoye, S., Mank, H. and Daudin, B., Appl. Phys. Lett. **85**, 1421 (2004).

[12] Neugebauer, J., Zywietz, T.K., Scheffler, M., Northrup, J.E., Chen, H. and Feenstra, R.M., Phys. Rev. Lett. **90**, 056101 (2003).

[13] Lischka, K., phys. stat. sol. (b) **202**, 673 (1997).

[14] Yang, H., Brandt, O. and Ploog, K., J. Electr. Mat. **25** (5), 787 (1996).

[15] Okumura, H., Ohta, K., Feuillet, G., Balakrishnan, K., Chichibu, S., Hamaguchi, H., Hacke, P. , Yoshida, S., J. Crystal Growth **178**, 113 (1997).

[16] Yang, H., Zheng, L.X., Li, J.B., Wang, X.J., Xu, D.P., Wang, Y.T., Hu, X.W. and Han, P.D., Appl. Phys. Lett. **74** (17), 2498 (1999).

[17] Ayers, J.E., J. Appl. Phys. **78**, 3724 (1995).

[18] Daudin, B., Feuillet, G., Hübner, J., Samson, Y., Widmann, F., Philippe, A., Bru-Chevallier, C., Guillot, G., Bustarret, E., Bentoumi G. and Deneuville, A., J. Appl. Phys. **84** (4), 2295 (1998).

[19] As, D.J., Schmilgus, F., Wang, C., Schöttker, B., Schikora, D. and Lischka, K., Appl. Phys. Lett. **70** (10), 1311 (1997).

[20] Ramirez-Flores, G., Navarro-Contreras, H., Lastras-Martinez, A., Powell R.C. and Greene, J.E., Phys. Rev. **B 50** (12), 8433 (1994).

[21] Wetzel, C., Fischer, S., Krüger, J., Haller, E.E., Molnar, R.J., Moustakas, T.D., Mokhov E.N. and Baranov, P.G., Appl. Phys. Lett. **68** (18), 2556 (1996).

[22] Zinov´ev, N.N., Andrianov, A.V., Averbukh, B.Y., Yaroshetskii, I.D., Cheng, T.S., Jenkins, L.C., Hooper, S.E., Foxon C.T. and Orton, J.W., Semicond. Sci. Technol. **10**, 1117 (1995).

[23] Liu, Z.X., Goñi, A.R., Syassen, K., Siegle, H., Thomsen, C., Schöttker, B., As, D.J. and Schikora, D., J. Appl. Phys. **86** (2), 929 (1999).

[24] Haynes, J.R., Phys. Rev. Lett. **4** (7), 361 (1960).

[25] Merz, C., Kunzer, M., Kaufmann, U., Akasaki, I. and Amano, H., Semicond. Sci. Technol. **11**, 712 (1996).

[26] Wu, J., Yaguchi, H., Onabe, K., Ito, R., Shiraki, Y., Appl. Phys. Lett. **71** (15), 2067 (1997).

[27] Fortz, B.E., O'Leary, S.K., Shur, M.S. and Eastman, J. Appl. Phys. **85**, 7727 (1999).

[28] Pugh, S.K., Dugdale, D.J., Brand, S. and Abram, R.A., Semicond. Sci. Technol. **14**, 23 (1999).

[29] Gallinat, C.S., Koblmüller, G., Brown, J.S., Bernardis, S. and Speck, J.S., Appl. Phys. Lett. **89**, 032109 (2006).

[30] Fu, S.P., Chen, T.T. and Chen, Y.F., Semicond. Sci. Technol. **21**, 244 (2006).

[31] Schörmann, J., As, D.J., Lischka, K.., Schley, P., Goldhahn, R., Li, S.F., Löffler, W., Hetterich, M., Kalt, H., Appl. Phys. Lett. **89**, 261903 (2006).

[32] Schley, P., Goldhahn, R., Napierala, C., Schörmann, J., As, D.J., Lischka, K., Feneberg, M., Thonke, K., Semicond. Sci. Technol. **23**, 055001 (2008).

[33] King, P.D.C., Veal, T.D., McConville, C.F., Fuchs, F., Furthmüller, J., Bechstedt, F., Schley, P., Goldhahn, R., Schörmann, J., As, D.J., Lischka, K., Mutó, D., Naoi, H., Nanishi, Y., Lu, H., Schaff, W.J., Appl. Phys. Lett. **91**, 092101 (2007).

[34] Bai, J., Wang, T. and Sakai, S., J. Appl. Phys. **88** (8), 4729 (2000).

[35] Li, S.F., As, D.J., Lischka, K., Pacheco-Salazar, D.G., Scolfaro, L.M.R., Leite, J.R., Cerdeira, F., Meneses, E.A., MRS Symp. Proc. Vol. **831**, E8.15 (2005).

[36] Calle, F., Naranjo, F.B., Fernandez, S., Sanchez-Garcia, M.A., Calleja E. and Munoz, E., *phys. stat. sol. (a)* **192** (2), 277 (2002).

[37] Daudin, B. and Widmann, F., J. Cryst. Growth **182**, 1 (1997)

[38] Lebedev, V., Cimalla, V., Kaiser, U., Foerster, Ch., Pezoldt, J., Biskupek J. and Ambacher, O., J. Appl. Phys. **97**, 114306 (2005)

[39] Schupp, T., Rossbach, G., Schley, P., Goldhahn, R., Lischka K. and As, D.J., phys. stat. sol. (c), (2009) (in press).

[40] Braun, W., [Applied RHEED], Springer Tracts in Modern Physics, Vol. **154**, Springer, Berlin, (1999)

[41] Holy, V., [High-Resolution X-Ray Scattering from Thin Films and Multilayers], Springer Tracts in Modern Physics, Vol. **149**, Springer, Berlin, (1999)

[42] Cobet, C., Goldhahn, R., Richter, W. and Esser, N. phys. stat. sol. (b), **246**, 1440 (2009).

[43] Goldhahn, R., Acta Physica Polonica A **104**, 123 (2003).

[44] Röppischer, M., Goldhahn, R., Rossbach, G., Schley, P., Cobet, C., Esser, N., Schupp, T., Lischka, K., and As, D.J., J. Appl. Phys. **106**, 076104 (2009).

[45] Leute, R.A.R., Feneberg, M., Sauer, R., Thonke, K., Thapa, S.B., Scholz, F., Taniyasu, Y. and Kasu, M., Appl. Phys. Lett. **95**, 031903 (2009).

[46] Bechstedt, F., Seino, K., Hahn, P.H. and Schmidt, W.G., Phys. Rev. B **72**, 245114 (2005).

[47] Schörmann, J., Potthast, S., As, D.J., Lischka, K., Appl. Phys. Lett. **89**, 131910 (2006)

[48] As, D.J., Potthast, S., Köhler, U., Khartchenko A. and Lischka, K., MRS Symp. Proc. Vol. **743,** L5.4 (2003)

[49] Craven, M.D., Waltereit, P., Speck, J.S. and DenBaars, S.P., Appl. Phys. Lett. **84**, 496 (2004).

[50] Grandjean, N., Damilano, B., Dalmasso, S., Leroux, M., Laügt, M. and Massies, J., J. Appl. Phys. **86**, 3714 (1999).

[51] DeCuir, Jr., E.A., Fred, E., Manasreh, M.O., Schörmann, J., As, D.J., Lischka, K., Appl. Phys. Lett. **91**, 041911 (2007).

[52] DeCuir, Jr., E.A., Manasreh, M.O., Tschumak, E., Schörmann, J., As, D.J. and Lischka, K., Appl. Phys. Lett. **92**, 201910 (2008).